PAPER

Synthesis and characterization of some novel tetrazole liquid crystals†

Muhammad Tariq,[ab] Shahid Hameed,[b] Ivan H. Bechtold,[c] Adailton J. Bortoluzzi[d] and Aloir A. Merlo*[a]

The synthesis and characterization of new 4-[(2-alkyl)-2H-tetrazol-5-yl]phenyl 4-alkyloxybenzoates (**5a–i**) and 5-{4-[(4-substituted)benzyloxy]phenyl}-2-alkyl-2H-tetrazoles (**7a–e**) are reported. The reported tetrazoles contain two alkyl chains (six to ten carbon atoms) except for **5h** and **7e** which have a chiral citronellyl group linked at the N-2 nitrogen atom of the tetrazole ring and **5i** having a bromine atom at the *para* position of benzoate. The regiochemistry in the alkylation step was established unequivocally by single-crystal X-ray analysis for **5a** and **5f**. The regioselectivity in the alkylation step was also confirmed by analysis of ^{13}C NMR chemical shifts of the C_5 carbon atom in the tetrazole ring and the methylene carbon atom vicinal to the nitrogen atom. The mesogenic behavior of the liquid crystals was characterized by polarizing optical microscopy (POM), differential scanning calorimetry (DSC) and X-ray diffraction (XRD) techniques. The tetrazolyl benzoates **5a–h** show a nematic mesophase. The lengthening of alkyl chains favors the appearance of the smectic mesophase. For instance, **5g** displayed nematic and smectic C mesophases, while **5h** which has the chiral citronellyl group displayed nematic and smectic A mesophases. Tetrazoles **7a–e** did not show mesomorphic behavior mainly due to replacement of the carbonyl by a methylene group.

Introduction

Liquid Crystals (LCs) containing heterocyclic rings are of crucial importance in the design and synthesis of novel advanced functional materials. Liquid-crystalline phases, polarity, geometry, luminescence and other molecular properties may be varied through the introduction of heteroatoms.[1] Among heterocyclic systems, 5-membered heterocyclic rings are of great importance as core units in thermotropic liquid crystals due to their ability to impart lateral and longitudinal dipoles with changes in molecular shape. These materials have potential for use in applications such as spatial light modulation,[2] optical information storage,[3] organic thin-film transistors,[4,5] fast-switching ferroelectric materials,[6] fluorescent probes for the detection and analysis of biomolecules.[7] Furthermore, luminescent liquid crystals are of great interest since their self-organizing properties can be exploited to improve device performance and to achieve linearly polarized light.[8]

Heterocyclic compounds containing a high level of nitrogen atoms have gained much importance from the academic perspective to the technological application level.[9] For instance, these unnatural N-heterocyclic compounds like 1,2,3-triazoles exhibit high levels of biological activity.[10] They also have great potential in materials chemistry for the production of dyes, corrosion inhibitors, photostabilizers and photographic materials.[11] Some 1,2,3-triazole derivatives exhibit fluorescence, as studied by Wang *et al.*[12] in addition to their bioconjugation and bioimaging applications.

In recent years, tetrazole heterocyclics have got much significance in coordination chemistry[13,14] due to their ability to act as a ligand. Tetrazole derivatives have been significant in material applications such as speciality explosives, information recording systems, rocket propellants and in agrichemical applications. In particular tetrazole derivatives can be used as an alternative to the carboxylic moiety in drug design due to their resistance to many biological metabolic degradation pathways.[15] In this regard several compounds have been synthesized and tested for their pharmaceutical or medicinal purposes.[16]

In the liquid crystals field there are a few reports about the synthesis of tetrazoles and their LC properties.[17–19] Our synthetic efforts have showed that the tetrazole ring can be used as an alternative building block to prepare a new and more anisotropic class of LCs such as biaxial nematic or ferroelectric smectic C mesophases. The aim of our present work is to report

[a]Institute of Chemistry, UFRGS, Porto Alegre, RS, Brazil. E-mail: aloir.merlo@ufrgs.br; Fax: +55 51 3308 7304; Tel: +55 51 3308 7316

[b]Department of Chemistry, Quaid-i-Azam University, Islamabad-45320, Pakistan

[c]Department of Physics, UFSC, Florianópolis, SC, Brazil

[d]Department of Chemistry, UFSC, Florianópolis, SC, Brazil

† Electronic supplementary information (ESI) available: NMR spectra, DSC files, and mesophase pictures. CCDC 932470 and 932471. For ESI and crystallographic data in CIF or other electronic format see DOI: 10.1039/c3tc30966e

This journal is © The Royal Society of Chemistry 2013

J. Mater. Chem. C, 2013, **1**, 5583–5593 | **5583**

the synthesis of two new series of alkylated *N*-2 tetrazole derivatives and investigate their liquid-crystalline behaviour. In this work, the tetrazole ring was built by 1,3-dipolar addition of the azide anion (N_3^-) to an aryl nitrile. The regioselectivity during the alkylation step was established unequivocally by single crystal X-ray analysis for the two of the LC molecules, **5a** and **5f**, respectively.

Results and discussion

Synthesis

The preparation of ester **5a–i** and ether tetrazoles **7a–e** is outlined in Scheme 1. The key intermediate **3** was prepared in four steps starting from cyanophenol **1** by the use of protection and deprotection strategy of the phenol group to prevent the *O*-alkylation reaction. The tetrazole ring was constructed by the [3 + 2] 1,3-dipolar cycloaddition of the azide anion to cyanophenol **1** followed by the acetylation reaction of phenol functionality to obtain **2** in 51% yield over two steps. The alkylation reaction of **2** with alkylbromides gave the corresponding *N*-2 alkylated tetrazoles which on basic hydrolysis afforded **3** in good yields.

The compounds **5a–f** were obtained by esterification reaction between the freshly prepared phenol and 4-*n*-alkoxybenzoic acid **4a–e**[20] in the range of 21–34% yield. For **5i** the alkoxy group (RO) was replaced by the bromine atom. The compounds **7a–e** were

obtained by the alkylation of phenol **3** with a selected group of benzyl bromides **6a–d** in 45–55% yield.

The alkylation reaction of tetrazole **2** can render two regioisomers: alkylation may occur at *N*-1 and *N*-2 of the tetrazole ring. The regioselectivity depends on the reaction conditions, the nature of the alkylating agent and the influence of the substituent at the C-5 carbon atom of the tetrazole ring. *N*-1 and *N*-2 isomeric tetrazoles can be readily distinguishable by their ^{1}H and ^{13}C NMR spectra. According to Butler[21] and others,[18,22] C-5 resonates at *ca.* δ 150 ppm for *N*-1 tetrazole and at *ca.* δ 160 ppm for *N*-2 tetrazole. Further, the resonance line for ^{13}C of the methylene carbon atom of the alkyl chain on the nitrogen atom is shifted down field in the *N*-2 product (*ca.* δ 50 ppm) compared to the *N*-1 product (*ca.* δ 45 ppm). In our case the chemical shift of C-5 and the methylene carbon atom appeared at 163.6 and 53.2 ppm respectively confirming the alkylation at
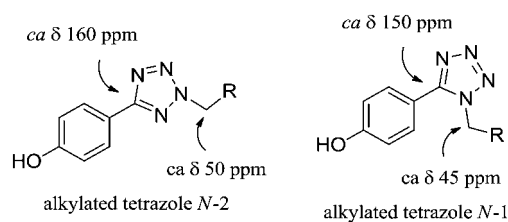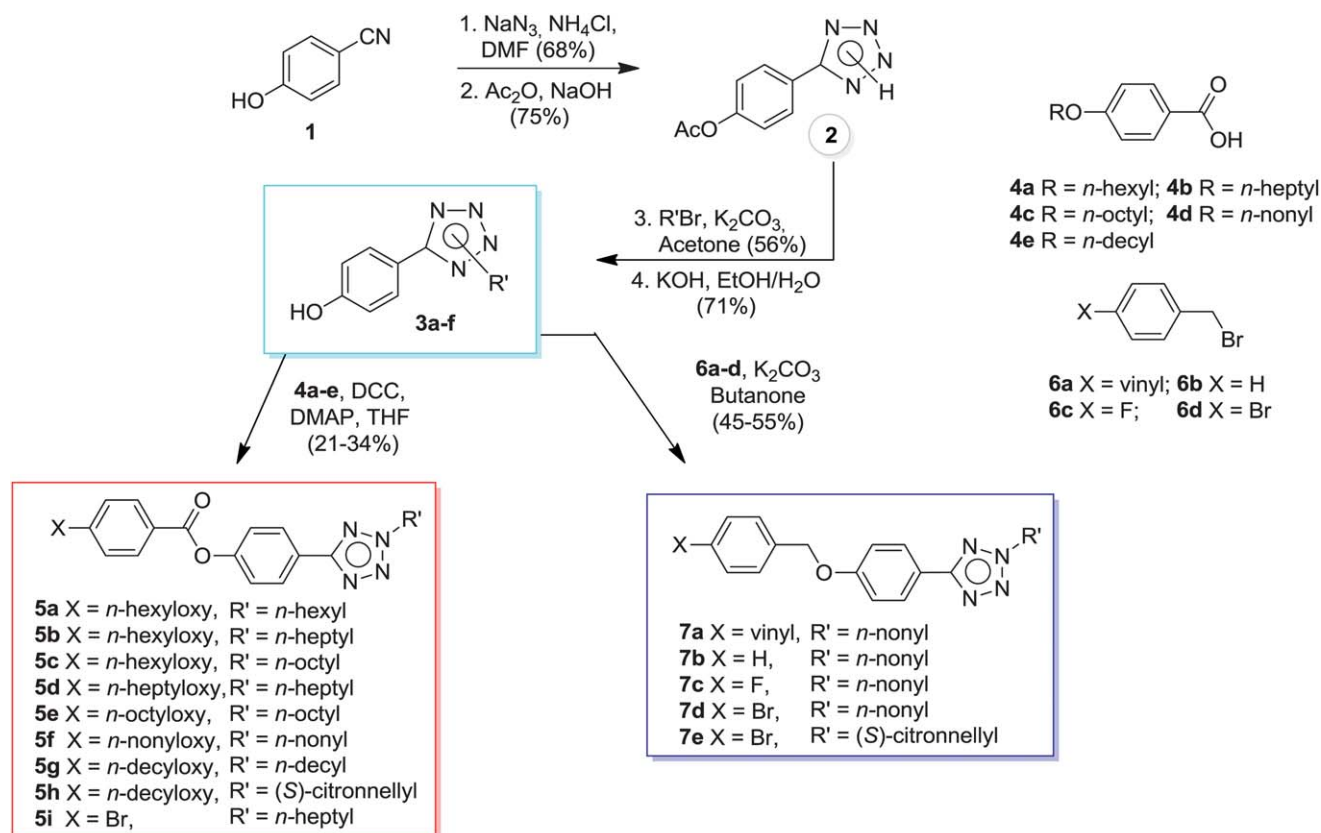

Fig. 1 ^{13}C NMR chemical shifts of the *N*-2 and *N*-1 tetrazole and methylene carbon atoms.

Scheme 1 Synthesis of tetrazoles **5a–f** and **7a–e**.

the N-2 nitrogen atom. The ^{13}C chemical shift values for tetrazole and methylene carbon atoms in **3** for N-2 (left) and its regioisomer N-1 (right) are shown in Fig. 1. The alkylation was also confirmed by analysing the crude product by GC-MS where there was no peak observed for the N-1 alkylated tetrazole.

The regiochemistry of the tetrazole derivatives was also established unequivocally by single crystal X-ray structure analysis. It confirms (Fig. 2 and 3) that alkylation proceeds regioselectively at N-2 rather than N-1.

The single crystal X-ray diffraction studies for **5a** and **5f** were accomplished successfully showing distinct conformation behavior of alkyl chains linked to the tetrazolyl moiety. The structure of **5a** shows that the conformation is folded with respect to terminal alkyl chains on N-2 of tetrazole (Fig. 2a) whereas for **5f** the carbon atoms of the alkyl chain are in zig–zag conformation (extended conformation, Fig. 3a). The n-hexyl chain bonded to the tetrazole ring in **5a** is pointed out of the main plane formed by five and six-membered rings of the central moiety. In addition, the packing analysis shows molecules stacked along the [100] direction forming piles related by the center of symmetry. Compound **5f** crystallizes in the space group $P\bar{1}$ with two molecules in the asymmetric unit (Fig. 3b). The molecules of **5f** show only different conformational arrangement, where the main features are the dihedral angles between the main planes of the phenyl rings of 54.75(8)° for C_{11}–C_{16}/C_{21}–C_{26} rings and 56.33(8)° for C_{61}–C_{66}/C_{71}–C_{76} rings for each independent molecule. The relative orientation of the carboxyl group and the phenyl group to which it is bonded is almost coplanar with a dihedral angle of 177.91(15)° for the O_2–C_2–C_{21}–C_{26} bonds of **5a** while conformations of **5f** display
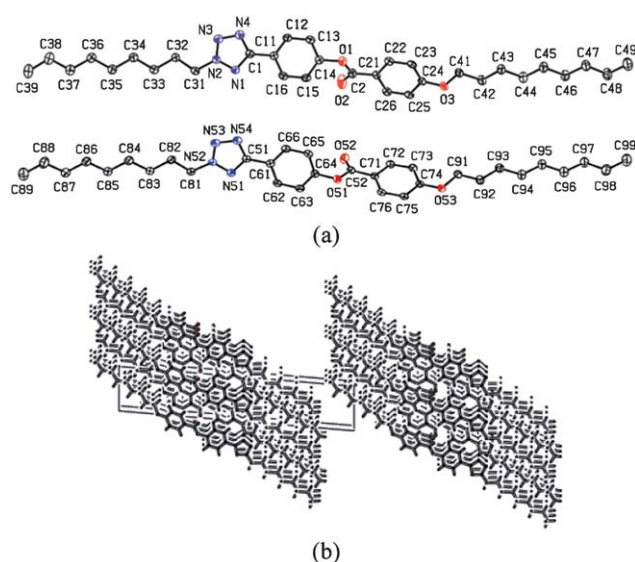

Fig. 3 (a) Molecular structure of **5f** showing the labelling scheme. Ellipsoids are represented at 40% probability level. H atoms were omitted for clarity. (b) Packing of **5f** along the crystallographic b axis.

two distinct orientations of the carboxyl group with a small deviation from coplanarity with dihedral angles of 164.4(4)° and 166.7(3)° for O_2–C_2–C_{21}–C_{22} and O_{52}–C_{52}–C_{71}–C_{76}, respectively. The carboxyl group is the bridge between two aromatic groups which lie in two molecular planes. These planes are not coplanar and the twist angle around C_{sp2}–C=O is larger for **5a** than for **5f**. For example, the twist angle for **5a** is −100.88(15) for C_{15}–C_{14}–O_1–C_2 bonds and 72.2(4)° and −70.1(4)° for C_{15}–C_{14}–O_1–C_2 and C_{65}–C_{64}–O_{51}–C_{52} bonds of **5f**, respectively. As we stated above, the carboxyl group is coplanar to the phenyl ring but almost perpendicular to another tetrazolylphenyl moiety represented by the twist angle mentioned above.

The coplanarity is also observed for the alkoxy/phenyl group and the tetrazolyl/phenyl group for both **5a** and **5f** compounds with dihedral angles between them almost being near to 0°. However, for **5a** the deviation from coplanarity for the N_4–C_1–C_{11}–C_{16} atoms is higher where the dihedral angle is 11.5(2)°. The reason for this behavior is the folded conformation of alkyl chain. Unlike **5f** which has antiperiplanar arrangement for all carbon atoms including the N-1 atom of tetrazole for two molecules in the asymmetric unit, **5a** has a folded conformation of the alkyl chains on N-2 of tetrazole. The torsion angles for C_{32}–C_{31}–N_2–N_1 and C_{32}–C_{31}–N_2–N_3 atoms are 73.50(18)° and −104.58(17)° respectively. It is clearly seen that the rotamers associated with a set of atoms prefer to adopt a gauche-like conformation instead of antiperiplanar or synperiplanar conformation in the crystal state.

The origin of conformational preference of **5a** for a folded conformation and of **5f** for an extended conformation of alkyl chains remains uncertain in the crystal state. Both the compounds were exposed to the same experimental conditions to obtain a single crystal for X-ray analysis. We are speculating that conformational behavior observed in the crystal state in this study may have an influence on the mesogenic behavior. The population levels of conformers as noted for **5a** and **5f** in the crystal state
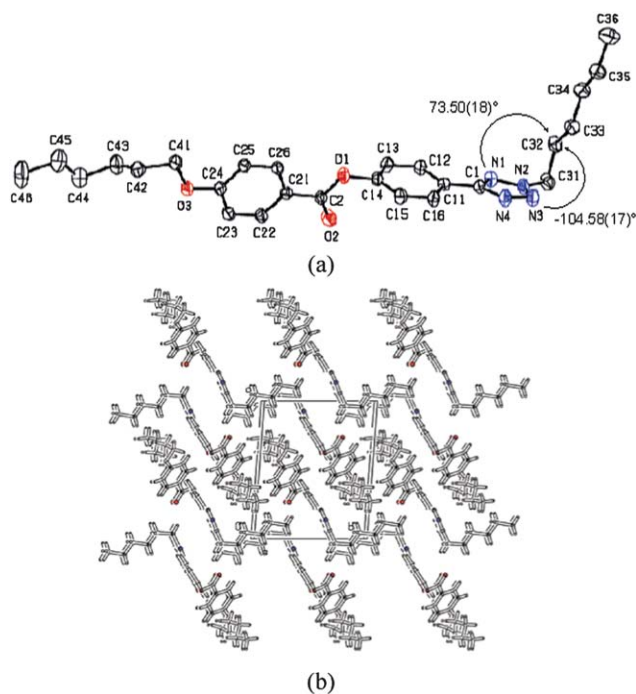

Fig. 2 (a) Molecular structures of **5a** showing the labelling scheme. Ellipsoids are represented at 40% probability level. H atoms were omitted for clarity. (b) Packing of **5a** along the crystallographic a axis.

could have an influence on the transition temperature associated with the crystal to mesophase and mesophase to isotropic phase. Upon slow heating and cooling cyles the more anisotropic conformation is favoured as the sample enters into the nematic phase.[23] As will be discussed in the liquid crystal properties section we have performed the DSC analysis at different rate conditions to get a separation of peaks related to the crystal to mesophase and mesophase to isotropic state transitions. The better separation of the peaks in DSC traces performed in this study was obtained under a slow cooling rate, usually 2 or 1 °C min^{-1}.

Liquid crystal properties

For all tetrazole LCs (**5a–h**) the phase transition temperatures and textures of the samples were acquired on the Mettler Toledo FP82HT hot stage combined with a FP90 controller and in conjunction with differential scanning calorimetry (DSC). The melting points for non-liquid crystal tetrazoles **5i** and **7a–e** were measured by polarizing optical microscopy (POM) using the hot stage system. The identification of the nematic mesophase for the compounds **5a–h** was made from the observation of typical planar texture with long dark lines, the so-called threads. These line singularities connect two defect points or form closed loops, see Fig. 4a and b, respectively. The planar thread-like texture is a characteristic of the liquid-crystalline nematic phase. At the early stage of cooling cycles a number of very small individual droplets are seen for all the LC samples. The low enthalpy values associated with transition of the mesophase (N) to the isotropic state (I) corroborate with this assignment (see Table 1). The dark shadows across Fig. 4a and b are imperfections of the glass. Bright yellowish color transition from the nematic mesophase to isotropic phase (black areas) at 78.5 °C upon heating is seen in Fig. 4c along with the loops and 2- and 4-fold singularity points for **5e**. Fig. 4d shows homeotropic texture (large black areas) and focal conic fan-like texture of the SmA phase for **5h** at 41 °C. Fig. 4e–h display a mesophase sequence for **5g** upon cooling. From the isotropic state **5g** enters the nematic phase with typical formation of dark lines characteristic of planar thread-like texture. As the temperature diminishes the planar texture takes place for whole sample **5g**. At *ca.* 71 °C the sample **5g** is left to stabilize and the texture of the nematic phase slowly transforms to *schlieren* texture. This is seen in the center of Fig. 4f where a slight change has occurred in the shape of the brushes, intensity and colour. Finally in Fig. 4g and h the nematic texture is completely transformed to a gray *schlieren* texture of the SmC mesophase (for additional pictures, see ESI†).

Transition temperatures (°C) and enthalpy values (kcal mol^{-1}) for tetrazolyl esters **5a–h** were collected using a DSC TA Q2000 or Q20 instrument with scan rates of 10 °C min^{-1}, 5 °C min^{-1} or 2 °C min^{-1}. Melting points (°C) for **5i** and ether tetrazoles **7a–e** were acquired by POM and are summarized in Table 1. Exceptionally for **5h** the data were collected at 1 °C min^{-1}. For compounds **5b**, **5c**, **5d** and **5f** the nematic to isotropic phase transitions were obtained by POM and enthalpy values were recorded as a sum of the crystal phase and nematic phase (Cr + N; Table 1). For these molecules the peaks observed in DSC traces could not be resolved even at a low rate of scans.
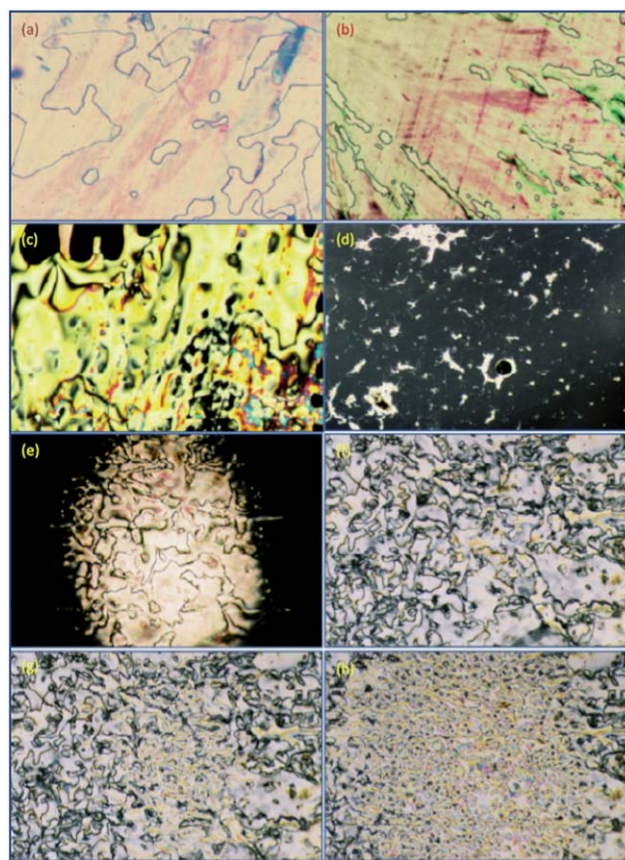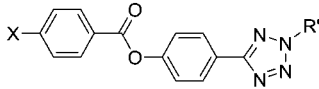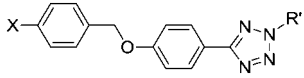

Fig. 4 Photomicrographs (×10) of the textures obtained by optical microscopy (a) and (b) thread-like texture associated with the nematic mesophase displayed by the compounds **5a** and **5d** at 76.0 °C and 72.0 °C respectively, upon heating; (c) transition to the isotropic state from the nematic phase for **5e** at 78.5 °C upon heating; (d) fan-shaped focal conic and homeotropic texture for the SmA mesophase displayed by **5h** at 41 °C; mesophase sequence for **5g** upon cooling – (e) schlieren texture of the nematic phase at 79 °C; (f), (g) and (h) schlieren texture of phase transition N → SmC transition at *ca.* 71 °C.

The POM pictures and DSC thermograms of **5a–g** showed that all samples display a stable nematic phase (N), with the mesophase range being larger upon cooling than upon heating. A supercooled nematic phase was observed for all the samples listed in Table 1 (see DSC traces in ESI†). For instance, **5a** melts to a nematic phase (N) at 68.5 °C and goes to the isotropic phase (I) at 78 °C, with $\Delta T = 9.5$ °C. Upon cooling, the sample enters into the nematic phase at 77.0 °C and 16.8 °C below the melting point the recrystallization takes place with $\Delta T = 25.3$ °C. The compound **5h** displays a chiral nematic phase (N*) due to the chiral citronellyl substituent bonded to the *N*-2 carbon atom on the tetrazole ring. Additionally, for **5g** and **5h** a monotropic smectic C and A phases (SmC, SmA) were observed, respectively. The smectogenic character of the last two compounds in this study is due to the increase in alkyl chain length on both sides of the mesogenic core. On the other hand upon heating **5h** goes directly to the isotropic phase at 60.0 °C. Upon cooling, the sample displays two peaks in DSC traces well below the melting point. These peaks were assigned to monotropic transition I → N* at 44.0 °C and N* → SmA* at 43.0 °C, respectively. The short mesophase range for **5h** probably is related to the

5586 | *J. Mater. Chem. C*, 2013, **1**, 5583–5593

This journal is © The Royal Society of Chemistry 2013

Table 1 Transition temperatures (°C) and enthalpy values (kcal mol^{-1}) for tetrazolyl esters **5a–i** and ether tetrazoles **7a–e**[a]

Entry	X	R′	Upon heating[b]/upon cooling[c]	ΔH (kcal mol^{-1})
5a	OC$_6$H$_{13}$	C$_6$H$_{13}$	Cr 68.5 N 78.0 I[d]/I 77.0 N 51.7 Cr	Cr 7.60 N 0.10 I
5b	OC$_6$H$_{13}$	C$_7$H$_{15}$	Cr 66.0 N 74.0[e] I/I 72.0[e] N 40.5 Cr	(Cr + N) 8.10 I
5c	OC$_6$H$_{13}$	C$_8$H$_{17}$	Cr 65.0 N 77.0[e] I/I 71.0[e] N 40.5 Cr	(Cr + N) 8.00 I
5d	OC$_7$H$_{15}$	C$_7$H$_{15}$	Cr 70.0 N 76.0[e] I/I 71.0[e] N 55.0 Cr	(Cr + N) 9.60 I
5e	OC$_8$H$_{17}$	C$_8$H$_{17}$	Cr 71.5 N 79.0 I[f]/I 78.5 N 50.0 Cr[f]	Cr 8.65 N 0.16 I
5f	OC$_9$H$_{19}$	C$_9$H$_{19}$	Cr 75.0 N 78.0[e] I/I 77.7 N 66.0 Cr[f]	(Cr + N) 11.0 I
5g	OC$_{10}$H$_{21}$	C$_{10}$H$_{21}$	Cr 76.0 SmC 79.0 N 81.0 I/I 80.0 N (71.0) SmC 65.0 Cr	[Cr (0.25[h])SmC] 11.0 N 0.31 I
5h	OC$_{10}$H$_{21}$	C$_{10}$H$_{19}$[g]	Cr 60.0 I/I 44.0 (N*) 43.0 (SmA*)[i] 23.0 Cr	Cr 8.70 I I 1.10[h] (N*+SmA*)[i] Cr 4.60[j]
5i	Br	C$_7$H$_{15}$	Cr 104–106 I/I 82 Cr	—

Entry	X	R′	Melting point (°C)
7a	Vinyl	C$_9$H$_{19}$	88–90
7b	Hydrogen	C$_9$H$_{19}$	75–78
7c	Fluor	C$_9$H$_{19}$	82–84
7d	Bromo	C$_9$H$_{19}$	92–94
7e	Bromo	C$_{10}$H$_{19}$[g]	52–54

[a] N = nematic mesophase; SmA = smectic A mesophase; SmC = smectic C mesophase; Cr = crystal phase; N*, SmA* and SmC* = chiral mesophases, respectively. [b] T_{onset} temperature from the crystal phase to nematic phase. [c] Supercooled nematic phase – transition temperature from the nematic phase to crystal phase obtained by DSC. [d] Transition temperatures was acquired by DSC TA Q20 at a rate of 5 °C min^{-1}. [e] Transition from the isotropic phase to nematic phase was acquired by POM. [f] Transition temperatures have been obtained by POM and DSC TA Q2000 at a rate of 2 °C min^{-1}. [g] (S)–CH$_2$CH$_2$CH(CH$_3$)(CH$_2$)$_2$CH=CMe$_2$ – chiral citronellyl substituent. [h] Value was obtained upon cooling. [i] Monotropic behaviour. [j] Value has been determined upon cooling.

unsaturated and branched citronellyl substituent which disfavors the appearance of enantiotropic behavior.[24,25]

While **5a–g** have a carboxyl group connecting the two aromatic rings which can help to stabilize the mesophase, compounds **7a–e** present a benzyl carbon atom as a connector group instead of the carboxyl group. The rotational process around the benzyl carbon atom is free to take place in **7a–e** contributing to the loss of linearity and planarity of the central part of the mesogenic core and also reducing the length : breadth ratio. Under these circumstances the mesophase formation is disfavored.

Chiral compounds such as **5h** and **7e** can be potential chiral dopant tetrazoles containing a citronellyl substituent with a low melting point. Compound **5i** is not a liquid crystal as it has a bromine atom as a substituent instead of the alkyl chain at the *para* position of benzoate ester.

For all compounds **5a–h** listed in Table 1, T_{onset} was taken as transition temperature associated with the melting of the crystal to nematic phase. The onset temperature of the melting process for these LC samples was independent of the heating rate. Phase transition from the nematic to isotropic phase upon heating at 10 °C min^{-1} is barely seen in DSC thermograms. As an example, a DSC trace for **5e** upon heating is shown in Fig. 5

where two peaks at 74.5 °C and 80.0 °C are seen at 10 °C min^{-1}, which are associated with the transition temperature peaks of Cr → N and N → I phases, respectively. The small peak at the right side of the main peak is almost covered by the main peak evidencing the existence of mesophase transition temperature.

According to the POM texture analysis that has been discussed above the peak at 80.0 °C was associated with the transition temperature from the nematic to isotropic state. Considering the scan rate at 10 °C min^{-1} makes it difficult to obtain the transition temperature associated with the nematic–isotropic phase in the DSC cycle and the non-symmetrical shape of the main peak, therefore, the DSC analysis was performed at 5 °C min^{-1}, 2 °C min^{-1} and in some cases at 1° min^{-1}. Under these conditions the base line in DSC traces is well-resolved as the rate is lowered progressively to 5 °C min^{-1} and 2 °C min^{-1}. As the rate approaches the low value the transition from the crystal to nematic and nematic to isotropic phase becomes clear and a symmetrical Gaussian peak emerges. Now the nematic mesophase range (ΔT = 7.5 °C) is available by DSC analysis. Interestingly, nematic to isotropic phase transition temperature could be acquired by POM but without the associated enthalpy. In addition, it is possible to observe that the shapes of DSC
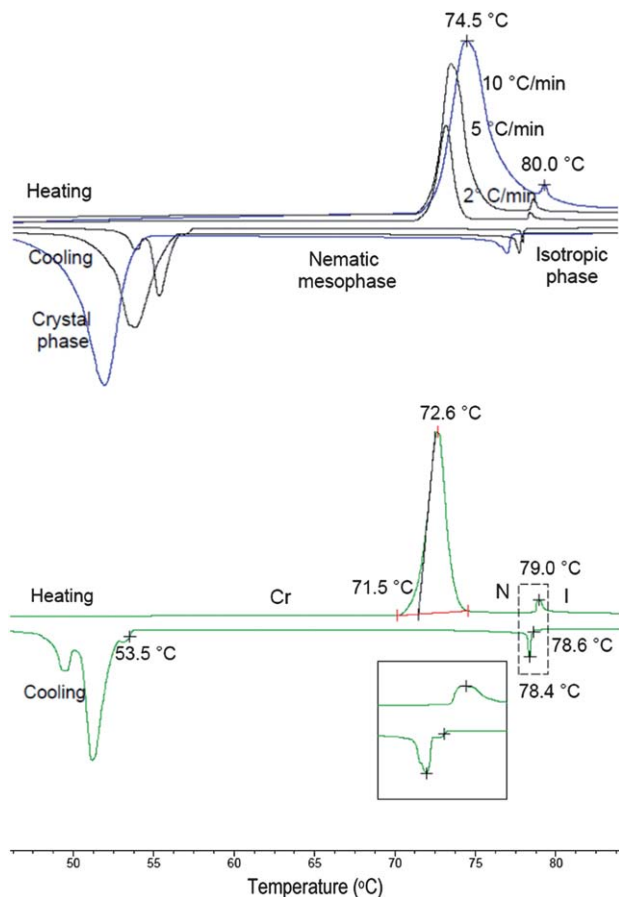
Fig. 5 A set of DSC traces for **5e** (10 °C, 5 °C and 2 °C min⁻¹, top) and a partial DSC trace at 2 °C min⁻¹ (bottom).

traces for most of the samples at 10 °C min⁻¹ are dependent on the rate of heating and cooling. This is clearly seen by the non-symmetrical shape at the right side of the main peak a *little tail* is seen at right side when the DSC traces are recorded at 10 °C min⁻¹ (see additional DSC for **5a**, **5d**, **5f** and **5g** in ESI†).

Fig. 5 illustrates a set of DSC thermograms recorded for compound **5e** at 10 °C, 5 °C min⁻¹ and 2 °C min⁻¹ (top) and a portion of the DSC trace for **5e** at 2 °C min⁻¹ (bottom). The mesophase range, well-defined shape peak and enthalpy values now are available from the DSC trace. It is worth mentioning that upon cooling two small steps are observable at 78.6 °C and 53.5 °C before the nematic mesophase formation and recrystallization takes place. The DSC trace performed at 2 °C min⁻¹ displays an additional small exothermic peak on the left side of the recrystallization peak. As mentioned in the Discussion section for conformation in the crystal phase, the transitional events as observed in the DSC thermograms could be related to reminiscent local orientational nematic order due to the fast scan rate and the non-equilibrium conditions. All samples in this study upon cooling enter the nematic phase by means of a number of very small individual droplets. The degree of supercooling of each droplet is different. This can be the origin of the DSC profile observed at the slow heating/cooling rate.[26]

In addition to the DSC analyses, a solid sample of **5c** was chosen and subjected to thermogravimetric analysis (TGA) (see

ESI†). The curve for the solid sample showed no apparent weight loss at 50–200 °C. Above this temperature, the TGA curve displayed three decomposition modes. The first weight loss (*ca.* 25.0%) that started at around 200–220 °C is related to elimination of the alkyl group attached to the tetrazole ring. The peak maximum to the first decomposition is 273.5 °C. The second mass loss process with *ca.* 28.0% is related to the alkoxy chain and is centered at around 330 °C. The final mass loss process (*ca.* 46.5%) is related to the complete degradation of the remaining compound with the maximum temperature of weight loss located around 430 °C.

X-ray results

The XRD experiment was carried out on compounds **5g** and **5h** to investigate the structure of the observed smectic phases. In both cases the patterns recorded contain a sharp peak in the low-angle region, together with the second order reflection, arising from the XRD on the smectic layers. The inter-layer spacing was obtained by applying Bragg's law to the first maximum. These peaks are associated with the Miller indices (001) and (002) and it is well known that the ratio of the distances associated with the Miller indices of the first peak confirms the smectic phase. Fig. 6 shows the pattern of compound **5h** in the SmA* phase at 30 °C, where the smectic order was confirmed. The inter-layer spacing of 37.8 Å is comparable to the molecular length of 36.2 Å (calculated considering the most extended molecular conformation). The broad diffuse band centered around 4.4 Å is related to the liquid-like order between the aliphatic chains. The interlayer spacing obtained for compound **5g** in the SmC phase at 66 °C was 33.8 Å and it is 3.0 Å lower than the molecular length. This reduction is related to the conformational disorder and/or to the inclination of the molecules in the smectic layers.[27]

Experimental

Materials and instrumentation

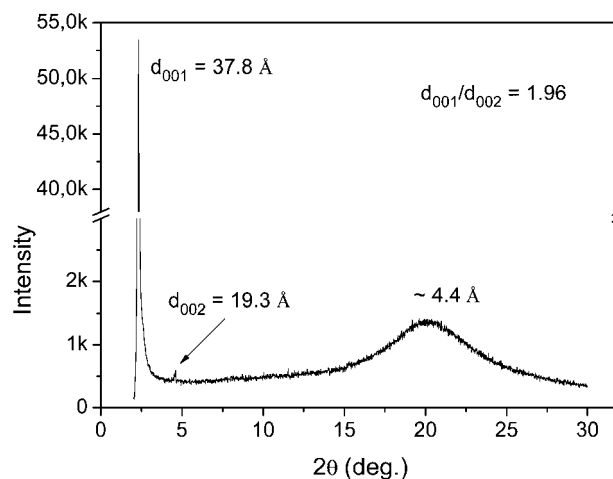All reagents used in the synthesis were purchased from Aldrich Chemical Company and the solvents received from Merck,

Fig. 6 X-ray diffraction pattern of compound **5h** in the SmA* phase at 30 °C. The ratio $d_{001}/d_{002} = 1.96$ confirms the smectic order.

Vetec, Baker, Fluka Chemika, Acros and Grupo Química were used as such. Solvents obtained from commercial sources were distilled before use. Infrared spectra were recorded on a Shimadzu Prestige 21 spectrometer using NaCl plates in the case of solids (nujol dispersions or neat) and as a thin film supported between NaCl plates in the case of liquids and are reported as wavenumber (cm^{-1}). Nuclear magnetic resonance spectra were obtained on Varian Inova 300 and Bruker 300 spectrometers. Chemical shifts are given in parts per million (δ) and are referenced from tetramethylsilane (TMS) in ^1H NMR spectra and from $CDCl_3$ or $(CD_3)_2CO$ in ^{13}C NMR spectra. Optical rotations were recorded on a Perkin-Elmer 341 polarimeter at the sodium D line. Low-resolution mass spectra were obtained with a Shimadzu GC-MS-QP5050 mass spectrometer interfaced with a Shimadzu GC-17A gas chromatograph equipped with a DB-17 MS capillary column. Elemental analyses were performed with a Perkin-Elmer model 2400 CHN elemental analyzer instrument. The melting points, phase transition temperatures and mesomorphic textures were taken using an Olympus BX43 microscope equipped with a Mettler Toledo FP82HT Hot Stage. The DSC analyses were obtained on a DSC Q2000 and Q20 TA Instruments. The X-ray diffraction (XRD) experiments were realized with the X'Pert-PRO (PANalytical) diffractometer using the linear monochromatic Cu Kα_1 beam ($\lambda = 1.5405$ Å), with an applied power of 1.2 kV A. The samples were prepared using procedures previously described in the literature.[28] The scans were performed in continuous mode from 2° to 30° (2θ angle) with the samples in the mesophase by cooling from the isotropic.

Preparation of 4-(2*H*-tetrazol-5-yl)phenyl acetate (2)

i   Cycloaddition reaction. To a solution of 4-cyanophenol (**1**) (5.0 g, 42 mmol) in 28 mL *N,N*-dimethyl formamide (DMF) was added sodium azide (11.0 g, 168 mmol) and ammonium chloride (9.0 g, 168 mmol). The mixture was stirred for 24 hours at 120 °C. The reaction mixture was cooled to room temperature, poured into 50 mL of ice cold water and acidified with concentrated HCl to pH 2. The precipitated solid was filtered and crystallized from ethanol giving 4-tetrazolyl phenol in 68% yield. $R_f = 0.23$ (*n*-hexane–ethyl acetate; 6 : 4); IR (neat, v_{max}, cm^{-1}): 3445, 3254, 2930, 2845, 1608. ^1H-NMR (300 MHz, $CDCl_3$): δ (ppm) 8.1 (2H, d, $J = 6.6$ Hz), 7.3 (2H, d, $J = 6.6$ Hz). ^{13}C-NMR (75 MHz, $CDCl_3$): δ (ppm) 169.4, 152.2, 127.3, 125.5, 122.6.

ii   Acylation reaction. 4-Tetrazolyl phenol (5.4 g, 33.3 mmol) was added to a sodium hydroxide solution (3 M, 27.6 mL), cooled in an ice bath and acetic anhydride (7.9 mL, 83.2 mmol) added dropwise along with ice (distilled water). The reaction mixture was vigorously stirred for 30 min and the precipitated solid was filtered, washed with cold water and crystallized from a water–methanol mixture. 4-(2*H*-Tetrazol-5-yl)phenyl acetate (**2**) was obtained as a white solid in 58% yield. $R_f = 0.33$ (*n*-hexane–ethyl acetate; 6 : 4); IR (neat, v_{max}, cm^{-1}): 3075, 2938, 2844, 1758, 1613, 1200. ^1H-NMR (300 MHz, $CDCl_3$): δ (ppm) 8.1 (2H, d, $J = 6.6$ Hz), 7.4 (2H, d, $J = 6.6$ Hz), 2.3 (3H, s). ^{13}C-NMR (75 MHz, $CDCl_3$): δ (ppm) 169.0, 158.0, 153.0, 128.0, 125.2, 122.4, 22.9.

General method for the synthesis of 4-[(2-alkyl)-2*H*-tetrazol-5-yl]phenyl acetate

A mixture of 4-(2*H*-tetrazol-5-yl)phenyl acetate (**2**) (2.50 g, 12 mmol), alkyl halide (12 mmol) and anhydrous K_2CO_3 (1.65 g, 12 mmol) in 30 mL acetone was refluxed for 48 h. The reaction mixture was cooled to room temperature and filtered to remove K_2CO_3. The solvent was removed at low pressure and the product was crystallized from ethanol.

4-[(2-Octyl-2*H*-tetrazol-5-yl]phenyl acetate. Yield: 40%; white solid; $R_f = 0.86$ (*n*-hexane–ethyl acetate; 7 : 3); IR (neat, v_{max}, cm^{-1}): 2952, 2851, 1758, 1207, 1613, 918. ^1H-NMR (300 MHz, $CDCl_3$): δ (ppm) 8.2 (2H, d, $J = 6.6$ Hz), 7.2 (2H, d, $J = 6.6$ Hz), 4.6 (2H, t, $J = 5.4$ Hz), 2.3 (3H, s), 2.1 (2H, quint, $J = 5.4$ Hz), 1.8–1.3 (10H, m), 0.9 (3H, t, $J = 5.1$ Hz). ^{13}C-NMR (75 MHz, $CDCl_3$): δ (ppm) 169.4, 164.5, 152.3, 128.2, 125.4, 122.3, 53.4, 31.8, 29.5, 29.2, 29.0, 26.5, 22.8, 21.4, 14.2.

4-[(2-Heptyl)-2*H*-tetrazol-5-yl]phenyl acetate. Yield: 29%; white solid; $R_f = 0.68$ (*n*-hexane–ethyl acetate; 7 : 3); IR (neat, v_{max}, cm^{-1}): 2916, 2851, 1765, 1200, 1605, 911. ^1H-NMR (300 MHz, $CDCl_3$): δ (ppm) 8.2 (2H, d, $J = 8.7$ Hz), 7.2 (2H, d, $J = 8.7$ Hz), 4.6 (2H, t, $J = 7.2$ Hz), 2.3 (3H, s), 2.1 (2H, quint, $J = 5.4$ Hz), 1.4–1.3 (8H, m), 0.8 (2H, q, $J = 6.3$ Hz). ^{13}C-NMR (75 MHz, $CDCl_3$): δ (ppm) 169.23, 164.33, 152.13, 128.08, 125.29, 122.16, 53.47, 31.56, 29.74, 29.41, 29.34, 22.54, 21.21, 14.06.

4-[(2-Hexyl)-2*H*-tetrazol-5-yl]phenyl acetate. Yield: 31%; white solid; $R_f = 0.69$ (*n*-hexane–ethyl acetate; 7 : 3); IR (neat, v_{max}, cm^{-1}): 2945, 2866, 1750, 1207, 1620, 918. ^1H-NMR (300 MHz, $CDCl_3$): δ (ppm) 8.2 (2H, d, $J = 6.6$ Hz), 7.2 (2H, d, $J = 6.6$ Hz), 4.6 (2H, t, $J = 5.4$ Hz), 2.3 (3H, s), 2.1 (2H, quint, $J = 5.4$ Hz), 1.4–1.2 (6H, m), 0.9 (3H, t, $J = 5.1$ Hz). ^{13}C-NMR (75 MHz, $CDCl_3$): δ (ppm) 169.2, 164.3, 152.1, 128.5, 125.2, 122.1, 53.2, 31.0, 29.3, 26.0, 22.4, 21.1, 13.9.

4-[(2-Nonyl)-2*H*-tetrazol-5-yl]phenyl acetate. Yield: 51%; white solid; $R_f = 0.74$ (*n*-hexane–ethyl acetate; 7 : 3); IR (neat, v_{max}, cm^{-1}): 2916, 2859, 1751, 1215, 1613, 918. ^1H-NMR (300 MHz, $CDCl_3$): δ (ppm) 8.2 (2H, d, $J = 6.6$ Hz), 7.2 (2H, d, $J = 6.6$ Hz), 4.6 (2H, t, $J = 6.6$ Hz), 2.3 (3H, s), 2.1 (2H, quint, $J = 5.2$ Hz), 1.4–1.3 (12H, m), 0.9 (3H, t, $J = 5.1$ Hz). ^{13}C-NMR (75 MHz, $CDCl_3$): δ (ppm) 169.2, 164.3, 152.1, 128.1, 125.3, 122.2, 53.3, 31.8, 29.4, 29.3, 29.2, 28.9, 26.4, 22.6, 21.2, 14.1.

4-[(2-Decyl)-2*H*-tetrazol-5-yl]phenyl acetate. Yield: 56%; white solid; $R_f = 0.73$ (*n*-hexane–ethyl acetate; 7 : 3); IR (neat, v_{max}, cm^{-1}): 2916, 2851, 1750, 1222, 1614, 918. ^1H-NMR (300 MHz, $CDCl_3$): δ (ppm) 8.2 (2H, d, $J = 6.6$ Hz), 7.3 (2H, d, $J = 6.6$ Hz), 4.6 (2H, t, $J = 5.4$ Hz), 2.3 (3H, s), 2.1 (2H, quint, $J = 5.4$ Hz), 1.4–1.3 (14H, m), 0.9 (3H, t, $J = 7.0$ Hz). ^{13}C-NMR (75 MHz, $CDCl_3$): δ (ppm) 169.2, 164.3, 152.1, 128.5, 125.2, 122.1, 53.3, 31.8, 29.6, 29.4, 29.2, 28.8, 26.3, 22.6, 21.2, 14.1.

(*S*)-(+)-4-[2-(3,7-Dimethyloct-6-enyl)-2*H*-tetrazol-5-yl]phenyl acetate. Yield: 60%; oily liquid; $R_f = 0.57$ (*n*-hexane–ethyl acetate; 7 : 3); ^1H-NMR (300 MHz, $CDCl_3$): δ (ppm) 8.2 (2H, d, $J = 9.3$ Hz), 7.2 (2H, d, $J = 8.7$ Hz), 5.1 (1H, t, $J = 5.4$ Hz), 4.6 (2H, t, $J = 5.2$ Hz), 2.3 (3H, s), 1.7–0.9 (17H, m). ^{13}C-NMR (75 MHz, $CDCl_3$): δ (ppm) 169.0, 164.1, 152.0, 131.5, 127.9, 125.1, 124.0, 122.0, 53.3, 36.5, 36.1, 29.7, 25.6, 25.1, 21.0, 18.9, 17.5.

General method for the deprotection reaction

4-[(2-Alkyl)-2*H*-tetrazol-5-yl]phenyl acetate (**2**) (3.1 mmol) was added to 20 mL methanol followed by addition of KOH (0.173 g, 3.1 mmol) in 5 mL water in a 100 mL round bottomed flask and refluxed for 12 hours. The mixture was cooled to room temperature, filtered and concentrated through rotary evaporator. The mixture was poured onto 100 g of ice and acidified with concentrated HCl to pH 2. The precipitated solid was filtered and purified by crystallization from ethanol.

4-[(2-Hexyl)-2*H*-tetrazol-5-yl]phenol (3a). Yield: 80%; white solid; $R_f = 0.71$ (*n*-hexane–ethyl acetate; 7 : 3); IR (neat, v_{max}, cm^{-1}): 3292, 2930, 1620, 853. ^{1}H-NMR (300 MHz, CDCl$_3$): δ (ppm) 8.0 (2H, d, $J = 6.6$ Hz), 6.9 (2H, d, $J = 6.6$ Hz), 4.7 (2H, t, $J = 5.4$ Hz), 2.1 (2H, quint, $J = 5.4$ Hz), 1.4–1.3 (8H, m), 0.9 (3H, t, $J = 5.2$ Hz). ^{13}C-NMR (75 MHz, CDCl$_3$): δ (ppm) 164.8, 157.7, 128.6, 119.9, 115.9, 53.2, 31.1, 29.4, 26.1, 22.4, 13.9.

4-[(2-Heptyl)-2*H*-tetrazol-5-yl]phenol (3b). Yield: 67%; white solid; $R_f = 0.69$ (*n*-hexane–ethyl acetate; 7 : 3); IR (neat, v_{max}, cm^{-1}): 3155, 2938, 1613, 853. ^{1}H-NMR (300 MHz, CDCl$_3$): δ (ppm) 8.0 (2H, d, $J = 8.7$ Hz), 6.9 (2H, d, $J = 8.7$ Hz), 4.6 (2H, t, $J = 7.2$ Hz), 2.1 (2H, quint, $J = 5.4$ Hz), 1.4–1.3 (6H, m), 0.8 (3H, t, $J = 6.6$ Hz). ^{13}C-NMR (75 MHz, CDCl$_3$): δ (ppm) 164.8, 157.5, 128.5, 120.1, 115.8, 53.2, 31.5, 29.4, 28.5, 26.3, 22.5, 14.0.

4-[(2-Octyl)-2*H*-tetrazol-5-yl]phenol (3c). Yield: 54%; white solid; $R_f = 0.86$ (*n*-hexane–ethyl acetate; 7 : 3); IR (neat, v_{max}, cm^{-1}): 3163, 2930, 1620, 845. ^{1}H-NMR (300 MHz, CDCl$_3$): δ (ppm) 7.9 (2H, d, $J = 8.7$ Hz), 6.9 (2H, d, $J = 8.7$ Hz), 4.0 (2H, t, $J = 6.6$ Hz), 1.8 (2H, quint, $J = 7.2$ Hz), 1.6–1.3 (10H, m), 0.9 (3H, t, $J = 5.8$ Hz). ^{13}C-NMR (75 MHz, CDCl$_3$): δ (ppm) 165.2, 158.0, 128.8, 120.0, 116.1, 53.4, 31.9, 29.6, 29.2, 29.1, 26.6, 22.8, 14.3.

4-[(2-Nonyl)-2*H*-tetrazol-5-yl]phenol (3d). Yield: 87%; white solid; $R_f = 0.72$ (*n*-hexane–ethyl acetate; 7 : 3); IR (neat, v_{max}, cm^{-1}): 3163, 2924, 1613, 845. ^{1}H-NMR (300 MHz, CDCl$_3$): δ (ppm) 8.0 (2H, d, $J = 6.6$ Hz), 6.9 (2H, d, $J = 6.6$ Hz), 4.6 (2H, t, $J = 5.4$ Hz), 2.1 (2H, quint, $J = 5.4$ Hz), 1.4–1.3 (12H, m), 0.8 (3H, q, $J = 5.1$ Hz). ^{13}C-NMR (75 MHz, CDCl$_3$): δ (ppm) 164.9, 157.9, 128.5, 119.7, 115.9, 53.2, 31.8, 29.4, 29.3, 29.2, 28.9, 26.4, 22.6, 14.1.

4-(2-Decyl)-2*H*-tetrazol-5-yl]phenol (3e). Yield: 75%; white solid; $R_f = 0.85$ (*n*-hexane–ethyl acetate; 7 : 3); IR (neat, v_{max}, cm^{-1}): 3409, 2916, 1620, 845. ^{1}H-NMR (300 MHz, CDCl$_3$): δ (ppm) 8.1 (2H, d, $J = 6.9$ Hz), 7.0 (2H, d, $J = 6.6$ Hz), 4.6 (2H, t, $J = 5.4$ Hz), 1.8 (2H, quint, $J = 5.1$ Hz), 1.4–1.2 (14H, m), 0.9 (3H, t, $J = 5.1$ Hz). ^{13}C-NMR (75 MHz, CDCl$_3$): δ (ppm) 164.9, 160.8, 128.3, 119.9, 114.8, 53.1, 31.8, 29.6, 29.6, 29.5, 28.9, 26.4, 22.7, 18.5, 14.2.

(S)-(+)-4-[2-(3,7-Dimethyloct-6-enyl)-2*H*-tetrazol-5-yl]phenol (3f). Yield: 64%; white solid; $R_f = 0.71$ (*n*-hexane–ethyl acetate; 7 : 3); ^{1}H-NMR (300 MHz, CDCl$_3$): δ (ppm) 8.0 (2H, d, $J = 6.6$ Hz), 6.9 (2H, d, $J = 6.6$ Hz), 5.1 (1H, t, $J = 5.4$ Hz), 4.6 (2H, t, $J = 5.2$ Hz), 1.7–0.9 (17H, m). ^{13}C-NMR (75 MHz, CDCl$_3$): δ (ppm) 164.8, 157.7, 131.7, 128.6, 124.1, 119.9, 115.9, 51.4, 36.6, 36.3, 29.9, 25.7, 25.2, 19.1, 17.7. $[\alpha]^D = + 10$ (1.94, CH$_2$Cl$_2$).

General method for the synthesis of 4-[2-(alkyl)-2*H*-tetrazol-5-yl]phenyl 4-alkyloxybenzoate

To a solution of 4-[(2-alkyl)-2*H*-tetrazol-5-yl]phenol (**3a–f**) (1.42 mmol) in 20 mL of dry THF was added 4-*n*-alkoxybenzoic acid

(**4a–e**) (1.42 mmol), dicyclohexylcarbodiimide (0.31 g, 1.50 mmol) and *N,N*-dimethyl aminopyridine (0.02 g, 0.15 mmol). The reaction mixture was stirred at room temperature for 24 hours. The precipitated solid was filtered and solvent was evaporated under low pressure. The solids were purified by column chromatography (*n*-hexane–ethyl acetate 95 : 5).

4-[(2-Hexyl)-2*H*-tetrazol-5-yl]phenyl 4-hexyloxybenzoate (5a). Yield: 33%; white solid; $R_f = 0.74$ (*n*-hexane–ethyl acetate; 7 : 3); IR (neat, v_{max}, cm^{-1}): 2930, 2859, 1736, 1605, 1201, 888. ^{1}H-NMR (300 MHz, CDCl$_3$): δ (ppm) 8.2 (2H, d, $J = 9.0$ Hz), 7.3 (2H, d, $J = 9.0$ Hz), 6.9 (2H, d, $J = 9.0$ Hz), 4.6 (2H, t, $J = 7.2$), 4.1 (2H, t, $J = 6.6$ Hz), 2.1 (2H, quint, $J = 7.0$ Hz), 1.8 (2H, quint, $J = 7.3$ Hz), 1.5–1.3 (12H, m), 0.9–0.8 (6H, m). ^{13}C-NMR (75 MHz, CDCl$_3$): δ (ppm) 164.7, 164.4, 163.6, 152.6, 132.3, 128.0, 125.1, 122.4, 121.2, 114.3, 68.3, 53.2, 31.5, 31.0, 31.5–22.4, 14.0, 13.9. Elemental analysis (%) for C$_{26}$H$_{34}$N$_4$O$_3$ (450 g mol^{-1}): calcd C 69.31, H 7.61, N 12.43; found C 69.29, H 8.09, N 12.50%.

4-[(2-Heptyl)-2*H*-tetrazol-5-yl]phenyl 4-hexyloxybenzoate (5b). Yield: 37%; white solid; $R_f = 0.77$ (*n*-hexane–ethyl acetate; 7 : 3); IR (neat, v_{max}, cm^{-1}): 2922, 2852, 1734, 1603, 1257, 885. ^{1}H-NMR (300 MHz, CDCl$_3$): δ (ppm) 8.2 (2H, d, $J = 6.6$ Hz), 8.1 (2H, d, $J = 6.6$ Hz), 7.3 (2H, d, $J = 6.6$ Hz), 6.9 (2H, d, $J = 6.6$ Hz), 4.6 (2H, t, $J = 5.2$ Hz), 4.0 (2H, t, $J = 4.9$ Hz), 2.0 (2H, quint, $J = 5.4$ Hz), 1.8 (2H, quint, $J = 5.1$ Hz), 1.5–1.3 (20H, m), 0.9–0.8 (6H, m). ^{13}C-NMR (300 MHz, CDCl$_3$): δ (ppm) 164.7, 164.4, 163.6, 152.6, 132.3, 128.0, 125.1, 122.4, 121.2, 114.3, 68.3, 53.2, 31.7, 31.5, 29.4–22.6, 14.1, 14.0. Elemental analysis (%) for C$_{27}$H$_{36}$N$_4$O$_3$ (464 g mol^{-1}): calcd C 72.56, H 8.95, N 9.96; found C 72.84, H 8.97, N 9.86%.

4-[(2-Octyl)-2*H*-tetrazol-5-yl]phenyl 4-hexyloxybenzoate (5c). Yield: 40%; white solid; $R_f = 0.79$ (*n*-hexane–ethyl acetate; 7 : 3); IR (neat, v_{max}, cm^{-1}): 2927, 2856, 1725, 1603, 1252, 935. ^{1}H-NMR (300 MHz, CDCl$_3$): δ (ppm) 8.2 (2H, d, $J = 6.6$ Hz), 8.1 (2H, d, $J = 6.6$ Hz), 7.3 (2H, d, $J = 6.6$ Hz), 6.9 (2H, d, $J = 6.6$ Hz), 4.6 (2H, t, $J = 5.2$ Hz), 4.1 (2H, t, $J = 4.9$ Hz), 2.1 (2H, quint, $J = 5.4$ Hz), 1.8 (2H, quint, $J = 5.1$ Hz), 1.5–1.3 (22H, m), 0.9–0.8 (6H, m). ^{13}C-NMR (75 MHz, CDCl$_3$): δ (ppm) 164.7, 164.4, 163.6, 152.6, 132.3, 128.0, 125.1, 122.4, 121.2, 114.3, 68.3, 53.2, 31.7, 31.5, 29.4–22.6, 14.1, 14.0. Elemental analysis (%) for C$_{28}$H$_{38}$N$_4$O$_3$ (478 g mol^{-1}): calcd C 72.56, H 8.95, N 9.96; found C 72.84, H 8.97, N 9.86%.

4-[(2-Heptyl)-2*H*-tetrazol-5-yl]phenyl 4-heptyloxybenzoate (5d). Yield: 21%; white solid; $R_f = 0.60$ (*n*-hexane–ethyl acetate; 7 : 3); IR (neat, v_{max}, cm^{-1}): 2924, 2851, 1728, 1605, 1207, 896. ^{1}H-NMR (300 MHz, CDCl$_3$): δ (ppm) 8.2 (2H, d, $J = 8.4$ Hz), 8.2 (2H, d, $J = 8.4$ Hz), 7.3 (2H, d, $J = 8.1$ Hz), 6.9 (2H, d, $J = 8.4$ Hz), 4.6 (2H, t, $J = 7.2$ Hz), 4.1 (2H, t, $J = 6.6$ Hz), 2.1 (2H, quint, $J = 6.9$ Hz), 1.8 (2H, quint, $J = 6.9$ Hz), 1.5–1.2 (16H, m), 0.9–0.8 (6H, m). ^{13}C-NMR (75 MHz, CDCl$_3$): δ (ppm) 164.6, 164.4, 163.6, 152.5, 132.3, 128.0, 125.0, 122.3, 121.2, 114.3, 68.3, 53.2, 31.7, 31.5, 29.7–22.5, 14.1, 14.0. Elemental analysis (%) for C$_{28}$H$_{38}$N$_4$O$_3$ (478 g mol^{-1}): calcd C 70.26, H 8.00, N 11.71; found C 70.64, H 8.43, N 11.02%.

4-[(2-Octyl)-2*H*-tetrazol-5-yl]phenyl 4-octyloxybenzoate (5e). Yield: 28%; white solid; $R_f = 0.71$ (*n*-hexane–ethyl acetate; 7 : 3); IR (neat, v_{max}, cm^{-1}): 2916, 2851, 1728, 1599, 1200, 896. ^{1}H-NMR (300 MHz, CDCl$_3$): δ (ppm) 8.2 (2H, d, $J = 8.4$ Hz), 8.1 (2H, d, $J = 8.7$ Hz), 7.3 (2H, d, $J = 8.1$ Hz), 6.9 (2H, d, $J = 8.7$ Hz), 4.6 (2H, t, $J = 7.2$ Hz), 4.0 (2H, t, $J = 6.6$ Hz), 2.1 (2H, quint, $J = 7.2$ Hz), 1.8

(2H, quint, J = 6.9 Hz), 1.5–1.3 (20H, m), 0.9–0.8 (6H, m). ^{13}C-NMR (75 MHz, CDCl$_3$): δ (ppm) 164.7, 164.4, 163.6, 152.6, 132.3, 128.0, 125.1, 122.4, 121.2, 114.3, 68.3, 53.2, 31.8, 31.7, 29.3–22.6, 14.1, 14.0. Elemental analysis (%) for C$_{30}$H$_{42}$N$_4$O$_3$ (506 g mol^{-1}): calcd C 71.11, H 8.36, N 11.06; found C 70.81, H 8.76, N 10.66%.

4-[(2-Nonyl)-2H-tetrazol-5-yl]phenyl 4-nonyloxybenzoate (5f). Yield: 18%; white solid; R_f = 0.62 (n-hexane–ethyl acetate; 7 : 3); IR (neat, v_{max}, cm^{-1}): 2916, 2851, 1728, 1599, 1200, 896. ^{1}H-NMR (300 MHz, CDCl$_3$): δ (ppm) 8.2 (2H, d, J = 8.4 Hz), 8.1 (2H, d, J = 8.4 Hz), 7.3 (2H, d, J = 8.4 Hz), 6.9 (2H, d, J = 8.7 Hz), 4.6 (2H, t, J = 7.1 Hz), 4.6 (2H, t, J = 7.1 Hz), 4.0 (2H, t, J = 6.6 Hz), 2.1 (2H, quint, J = 7.0 Hz), 1.8 (2H, quint, J = 6.6 Hz), 1.5–1.2 (24H, m), 0.9–0.8 (6H, m). ^{13}C-NMR (75 MHz, CDCl$_3$): δ (ppm) 164.7, 164.4, 163.7, 152.6, 132.4, 128.1, 125.1, 122.4, 121.3, 114.4, 68.4, 53.3, 31.9, 31.8, 29.5–22.7, 14.14, 14.12. Elemental analysis (%) for C$_{32}$H$_{46}$N$_4$O$_3$ (534 g mol^{-1}): calcd C 71.88, H 8.67, N 10.48; found C 71.51, H 9.04, N 10.46%.

4-[(2-Decyl)-2H-tetrazol-5-yl]phenyl 4-decyloxybenzoate (5g). Yield: 34%; white solid; R_f = 0.85 (n-hexane–ethyl acetate; 7 : 3); IR (neat, v_{max}, cm^{-1}): 2916, 2851, 1750, 1614, 1222, 918. ^{1}H-NMR (300 MHz, CDCl$_3$): δ (ppm) 8.2 (2H, d, J = 6.6 Hz), 8.2 (2H, d, J = 6.9 Hz), 7.4 (2H, d, J = 6.6 Hz), 7.0 (2H, d, J = 6.6 Hz), 4.7 (2H, t, J = 5.2 Hz), 4.1 (2H, t, J = 4.9 Hz), 2.1 (2H, quint, J = 5.2 Hz), 1.8 (2H, quint, J = 5.2 Hz), 1.5–1.3 (28H, m), 0.9–0.8 (6H, m). ^{13}C-NMR (75 MHz, CDCl$_3$): δ (ppm) 164.7, 164.4, 163.7, 152.6, 132.4, 128.1, 125.1, 122.4, 121.3, 114.4, 68.4, 53.3, 31.9, 31.8, 29.6–22.7, 14.1, 14.0. Elemental analysis (%) for C$_{34}$H$_{50}$N$_4$O$_3$ (562 g mol^{-1}): calcd C 72.56, H 8.95, N 9.96; found C 72.84, H 8.97, N 9.86%.

(S)-(+)-4-[2-(3,7-Dimethyloct-6-enyl)-2H-tetrazol-5-yl]phenyl 4-decyloxybenzoate (5h). Yield: 21%; white solid; R_f = 0.67 (n-hexane–ethyl acetate; 7 : 3); IR (neat, v_{max}, cm^{-1}): 2921, 2848, 1719, 1598, 1236, 890. ^{1}H-NMR (300 MHz, CDCl$_3$): δ (ppm) 8.2 (2H, d, J = 6.6 Hz), 8.2 (2H, d, J = 6.6 Hz), 7.3 (2H, d, J = 6.6 Hz), 6.9 (2H, d, J = 6.9 Hz), 5.1 (1H, t, J = 5.4 Hz), 4.7 (2H, t, J = 5.4 Hz), 4.0 (2H, t, J = 5.1 Hz), 1.8–0.8 (15H, m). ^{13}C-NMR (75 MHz, CDCl$_3$): δ (ppm) 164.6, 164.4, 163.6, 152.6, 132.3, 131.7, 128.0, 125.1, 124.1, 122.3, 121.2, 114.3, 68.3, 51.4, 36.6, 36.2, 31.8, 29.6–19.1, 17.6, 14.1. Elemental analysis (%) for C$_{34}$H$_{48}$N$_4$O$_3$ (560 g mol^{-1}): calcd C 72.82, H 8.94, N 9.99; found C 72.72, H 8.94, N 10.0%. [α]^D = + 28 (0.38, CH$_2$Cl$_2$).

4-(2-Heptyl-2H-tetrazol-5-yl)phenyl 4-bromobenzoate (5i). Yield: 32%; white solid; mp 104–106 °C; R_f = 0.82 (n-hexane–ethyl acetate; 7 : 3); IR (neat, v_{max}, cm^{-1}): 2919, 2857, 1745, 1610, 1218, 912. ^{1}H-NMR (300 MHz, CDCl$_3$): δ (ppm) 8.2 (2H, d, J = 6.6 Hz), 8.0 (2H, d, J = 6.6 Hz), 7.6 (2H, d, J = 6.3 Hz), 7.3 (2H, d, J = 6.6 Hz), 4.6 (2H, t, J = 5.4 Hz), 2.1 (2H, quint, J = 5.2 Hz), 1.5–1.3 (8H, m), 0.90 (3H, t, J = 5.4 Hz). ^{13}C-NMR (75 MHz, CDCl$_3$): δ (ppm) 164.4, 164.3, 163.7, 152.6, 131.4, 127.8, 125.3, 122.1, 121.3, 113.4, 53.3, 31.9, 31.8, 29.6, 28.7, 22.7, 14.1. Elemental analysis (%) for C$_{21}$H$_{23}$BrN$_4$O$_2$ (443 g mol^{-1}): calcd C 56.89, H 5.23, N 12.64; found C 56.60, H 5.35, N 12.76%.

General method for the synthesis of 5-[4-(4-substitutedbenzyloxy)phenyl]-2-nonyl-2H-tetrazole

A solution of 4-[(2-nonyl)-2H-tetrazol-5-yl]phenol (3d) (4.60 g, 16 mmol), 4-substituted benzyl halide 16 mmol and K$_2$CO$_3$ (2.20 g,

16 mmol) in butanone (40 mL) was refluxed for 12 hours. The mixture was cooled to room temperature, filtered and the solvent was evaporated at low pressure. The crude product was crystallized from ethanol to give the pure product.

5-[4-(4-Vinylbenzyloxy)phenyl]-2-nonyl-2H-tetrazole (7a). Yield: 32%; light brown solid; R_f = 0.71 (n-hexane–ethyl acetate; 7 : 3); IR (neat, v_{max}, cm^{-1}): 2913, 1614, 1252, 849. ^{1}H-NMR (300 MHz, CDCl$_3$): δ (ppm) 8.1 (2H, d, J = 6.6 Hz), 7.4 (2H, d, J = 6.3 Hz), 7.4 (2H, d, J = 6.3 Hz), 7.1 (2H, d, J = 6.9 Hz), 6.7 (1H, dd, J_{trans} = 13.2 Hz, J_{cis} = 8.1 Hz), 5.7 (1H, dd, J_{trans} = 13.2 Hz, J_{vic} = 0.6 Hz), 5.3 (1H, dd, J_{cis} = 8.1 Hz, J_{vic} = 0.6 Hz), 5.1 (2H, s), 4.6 (2H, t, J = 5.1 Hz), 2.0 (2H, quint, J = 5.4 Hz), 1.3–1.3 (12H, m), 0.8 (3H, t, J = 5.1 Hz). ^{13}C-NMR (75 MHz, CDCl$_3$): δ (ppm) 164.8, 160.3, 137.5, 136.4, 136.1, 128.3, 127.7, 126.4, 120.5, 115.2, 114.2, 69.8, 53.1, 31.8, 29.4, 29.3, 29.2, 28.9, 26.4, 22.6, 14.1.

4-[(4-Benzyloxy)phenyl]-2-nonyl-2H-tetrazole (7b). Yield: 60%; light brown solid; R_f = 0.62 (n-hexane–ethyl acetate; 7 : 3); IR (neat, v_{max}, cm^{-1}): 2921, 2845, 1608, 1237, 838. ^{1}H-NMR (300 MHz, CDCl$_3$): δ (ppm) 8.1 (2H, d, J = 6.6 Hz), 7.5–7.4 (5H, m), 7.3 (2H, d, J = 6.6 Hz), 5.1 (2H, s), 4.6 (2H, t, J = 5.3 Hz), 2.0 (2H, quint, J = 5.2 Hz), 1.3–1.2 (12H, m), 0.8 (3H, t, J = 5.1 Hz). ^{13}C-NMR (75 MHz, CDCl$_3$): δ (ppm) 164.8, 160.3, 136.6, 128.6, 128.3, 128.1, 127.5, 120.4, 115.2, 70.0, 53.1, 31.8, 29.4, 29.3, 29.1, 28.9, 26.4, 22.6, 14.1.

5-[4-(4-Flourobenzyloxy)phenyl]-2-nonyl-2H-tetrazole (7c). Yield: 45%; white solid; R_f = 0.77 (n-hexane–ethylacetate; 7 : 3); IR (neat, v_{max}, cm^{-1}): 2916, 2851, 1222, 918. ^{1}H-NMR (300 MHz, CDCl$_3$): δ (ppm) 8.1 (2H, d, J = 6.9 Hz), 7.4 (2H, d, J = 6.6 Hz), 7.1 (2H, d, J = 6.3 Hz), 7.1 (2H, d, J = 6.6 Hz), 5.1 (2H, s), 4.6 (2H, t, J = 5.4 Hz), 2.1 (2H, quint, J = 5.4 Hz), 1.6–1.2 (12H, m), 0.9 (3H, t, J = 4.8 Hz). ^{13}C-NMR (75 MHz, CDCl$_3$): δ (ppm) 164.8, 161.0, 160.1, 132.3, 132.2, 129.4, 128.3, 120.6, 115.7, 69.3, 53.1, 31.8, 29.4, 29.3, 29.2, 28.8, 26.4, 22.6, 14.1. Elemental analysis (%) for C$_{23}$H$_{29}$FN$_4$O (396 g mol^{-1}): calcd C 69.67, H 7.37, N 14.13; found C 69.47, H 7.68, N 14.18%.

5-[4-(4-Bromobenzyloxy)phenyl]-2-nonyl-2H-tetrazole (7d). Yield: 54%; white solid; R_f = 0.63 (n-hexane–ethyl acetate; 7 : 3); IR (neat, v_{max}, cm^{-1}): 2921, 2840, 1615, 1253, 841. ^{1}H-NMR (300 MHz, CDCl$_3$): δ (ppm) 8.1 (2H, d, J = 6.6 Hz), 7.5 (2H, d, J = 6.3 Hz), 7.3 (2H, d, J = 6.3 Hz), 7.1 (2H, d, J = 6.3 Hz), 5.1 (2H, s), 4.6 (2H, t, J = 5.4 Hz), 2.0 (2H, quint, J = 5.1 Hz), 1.3–1.3 (12H, m), 0.8 (3H, t, J = 5.1 Hz). ^{13}C-NMR (75 MHz, CDCl$_3$): δ (ppm) 164.7, 161.0, 135.6, 131.7, 129.0, 128.3, 122.0, 120.7, 115.1, 69.3, 53.1, 31.8, 29.4, 29.3, 29.1, 28.9, 26.4, 22.6, 14.1.

(S)-(+)-5-[4-(4-Bromobenzyloxy)phenyl]-2-(3,7-dimethyloct-6-enyl)-2H-tetrazole (7e). Yield: 45%; white solid; R_f = 0.60 (n-hexane–ethyl acetate; 7 : 3); IR (neat, v_{max}, cm^{-1}): 2977, 2848, 1623, 1252, 995. ^{1}H-NMR (300 MHz, CDCl$_3$): δ (ppm) 8.1 (2H, d, J = 6.6 Hz), 7.5 (2H, d, J = 6.3 Hz), 7.3 (2H, d, J = 6.3 Hz), 7.0 (2H, d, J = 6.9 Hz), 5.1 (2H, s), 4.6 (2H, t, J = 5.4 Hz), 2.1 (2H, quint, J = 5.1 Hz), 1.6–1.5 (19H, m). ^{13}C-NMR (75 MHz, CDCl$_3$): δ (ppm) 164.7, 160.1, 135.6, 131.8, 131.7, 129.1, 128.3, 124.2, 120.6, 115.7, 69.3, 51.4, 36.6, 36.3, 30.9, 29.9, 25.7, 25.2, 19.1, 17.7. Elemental analysis (%) for C$_{23}$H$_{29}$BrN$_4$O$_3$ (457 g mol^{-1}): calcd C 61.41, H 6.23, N 11.94; found C 61.14, H 6.21, N 11.62%. [α]^D = + 7 (1.2, CH$_2$Cl$_2$).

This journal is © The Royal Society of Chemistry 2013

J. Mater. Chem. C, 2013, 1, 5583–5593 | 5591

Single crystal X-ray crystallography

Crystals of **5a** and **5f** were selected from a homogeneous crystalline sample. X-ray diffraction data were measured on a Kappa-APEX II Duo diffractometer. Data collection was performed with the COLLECT software.[29] Integration and scaling of the intensities were carried out with the HKL DENZO-SCALEPACK software package.[30] Intensities were corrected for Lorentz and polarization effects. The structure was solved by direct methods[31] and refined by full-matrix least-squares on F^2.[32] All non-hydrogen atoms were refined with anisotropic displacement parameters. Hydrogen atoms bonded to C atoms were placed at their idealized positions using standard geometric criteria. The numbers in parenthesis are the esd (estimated standard deviation) values, once the dihedral angles were refined with MPLA instruction. Selected crystal data: compound **5a**: formula $C_{26}H_{34}N_4O_3$; FW 450.57; triclinic, space group $P\bar{1}$; $a = 8.8808(3)$ Å, $b = 10.9801(3)$ Å, $c = 13.8034(4)$ Å, $\alpha = 82.731(2)°$, $\beta = 72.7700(10)°$, $\gamma = 76.798(2)°$; $V = 1249.11(7)$ Å^3; $Z = 2$; $\rho_{calc} = 1.198$ Mg m^{-3}; $\mu = 0.079$ mm^{-1}; reflections collected = 28 779; unique = 8005 ($R_{int} = 0.0207$); GOOF (F^2) = 1.046; R_1 [$I > 2\sigma(I)$] = 0.0629, wR_2 (all data) = 0.2006. Compound **5f**: formula $C_{32}H_{46}N_4O_3$; FW 534.73; triclinic, space group $P1$; $a = 6.1964(4)$ Å, $b = 7.3745(4)$ Å, $c = 33.1004(18)$ Å, $\alpha = 93.630(3)°$, $\beta = 94.782(3)°$, $\gamma = 95.576(3)°$; $V = 1496.24(15)$ Å^3; $Z = 2$; $\rho_{calc} = 1.187$ Mg m^{-3}; $\mu = 0.077$ mm^{-1}; reflections collected = 17 024, unique = 10 061 ($R_{int} = 0.0328$); GOOF (F^2) = 1.057; R_1 [$I > 2\sigma(I)$] = 0.0661, wR_2 (all data) = 0.1794.

Conclusions

Two new sets of tetrazole derivatives **5a–i** and **7a–e** were synthesised and fully characterized. All the tetrazoles reported here contain two alkyl chains (six to ten carbon atoms) except for **5h** and **7e** which have a chiral citronellyl group linked at the N-2 nitrogen atom of the tetrazole ring. The regiochemistry in the alkylation step was established unequivocally by single-crystal X-ray analysis for **5a** and **5f**. In addition the regioselectivity was also confirmed by analysis of ^{13}C NMR chemical shifts of the both the C_5 carbon atom in the tetrazole ring and the methylene carbon atom vicinal to the nitrogen atom. The tetrazolyl benzoates **5a–h** show a nematic phase for all compounds. The lengthening of alkyl chains favors the appearance of the smectic mesophase as shown in **5g** which displays nematic and smectic C mesophases, while **5h** which has the chiral citronellyl group displayed a smectic A mesophase along with a nematic mesophase. Tetrazoles **7a–e** which have a methylene group as a linker instead of the carbonyl group do not show mesomorphic behavior. A preliminary discussion trying to correlate the conformation data obtained by single-crystal X-ray analysis of **5a** and **5f** and the DSC profile for LC samples at low heating/cooling rate cycles is presented. However, the question of how the liquid crystal properties are affected by the population levels of the conformers in the solid state remains open.

Acknowledgements

Notes and references

1 A. Seed, *Chem. Soc. Rev.*, 2007, **36**, 2046.

2 P. Bauerle, in *Oligothiophenes*, ed. K. Mullen and G. Wegner, Wiley-VCH, Weinheim, 1998.

3 H. Zhang, S. Shiino, A. Shishido, A. Kanazawa, O. Tsutsumi, T. Shiono and T. Ikeda, *Adv. Mater.*, 2000, **12**, 1336.

4 M. O'Neill and S. M. Kelly, *Adv. Mater.*, 2003, **15**, 1135.

5 Y. S. Park, D. Kim, H. Lee and B. Moon, *Org. Lett.*, 2006, **8**, 4699.

6 T. Geelhaar, *Ferroelectrics*, 1988, **85**, 329.

7 G. Barbarella, M. Zambianchi, O. Pudova, V. Paladini, A. Ventola, F. Cipriani, G. Gigli, R. Cingolani and G. Citro, *J. Am. Chem. Soc.*, 2001, **123**, 11600.

8 S. Torgova and A. Strigazzi, *Mol. Cryst. Liq. Cryst.*, 2002, **375**, 61; R. Cristiano, A. A. Vieira, F. Ely and H. Gallardo, *Liq. Cryst.*, 2006, **33**, 381; N. F. Marcelo, A. A. Vieira, R. Cristiano, H. Gallardo and I. H. Bechtold, *Synth. Met.*, 2009, **159**, 675; P. Alliprandini-Filho, G. F. Borges, W. B. Calixto, I. H. Bechtold, A. A. Vieira, R. Cristiano and H. Gallardo, *Chem. Phys. Lett.*, 2010, **487**, 263.

9 H. C. Kolb, M. G. Finn and K. B. Sharpless, *Angew. Chem., Int. Ed.*, 2001, **40**, 2004.

10 V. Calderone, *Curr. Med. Chem.*, 2002, **9**, 1385.

11 J. T. Sharp, in *Synthetic applications of 1,3-dipolar cycloaddition chemistry toward heterocycles and natural products*, Wiley-Interscience, New York, 2002, pp. 473–538.

12 K. Sivakumar, F. Xie, B. M. Cash, S. Long, H. N. Barnhill and Q. Wang, *Org. Lett.*, 2004, **6**, 4603.

13 E. Meyer, C. Zucco and H. Gallardo, *J. Mater. Chem.*, 1998, **8**, 1351.

14 H. Gallardo, I. M. Begnini, A. Neves and I. Vencato, *J. Braz. Chem. Soc.*, 2000, **11**, 274.

15 D. Zhenting, S. Changmei, L. Youqiang, W. Yin and L. Jing, *Int. J. Mol. Sci.*, 2012, **13**, 4696.

16 B. Akhlaghinia and S. Rezazadeh, *J. Braz. Chem. Soc.*, 2012, **23**, 2197; M. Baumann, I. R. Baxendale, S. V. Ley and N. Nikbin, *Beilstein J. Org. Chem.*, 2011, **7**, 442.

17 L. da Silva, H. Gallardo, R. F. Magnago and I. M. Begnini, *Mol. Cryst. Liq. Cryst.*, 2005, **432**, 1.

18 H. Gallardo, R. F. Magnago and A. Bortoluzzi, *Liq. Cryst.*, 2001, **28**, 1343.

19 D. R. dos Santos, A. G. S. de Oliveira, R. L. Coelho, I. M. Begnini, R. F. Magnago and L. da Silva, *ARKIVOC*, 2008, **xvii**, 157.

20 A. A. Merlo, H. Gallardo and T. R. Taylor, *Quim. Nova*, 2001, **24**, 354; U. B. Vasconcelos, E. Dalmolin and A. A. Merlo, *Org. Lett.*, 2005, **7**, 1027.

21 R. N. Butler, T. M. Mcevoy, F. C. Scott and J. C. Tobin, *Can. J. Chem.*, 1977, **55**, 1564.

22 A. D. Bond, A. Fleming, F. Kelleher, J. McGinleyc and V. Prajapati, *Tetrahedron*, 2006, **62**, 9577.

23 C. T. Imrie and G. R. Luckhurst, in *Handbook of Liquid Crystals*, ed. D. Demus, J. W. Goodby, G. W. Gray, H. W. Spiess and V. Vill, Wiley-VCH, Weinheim, 1998, pp. 801–833; C. T. Imrie and P. A. Henderson, *Chem. Soc. Rev.*, 2007, **36**, 2096–2124.

24 M. P. Aldred, P. Vlachos, D. Dong, S. P. Kitney, W. C. Tsoi, M. O'Neill and S. M. Kelly, *Liq. Cryst.*, 2005, **32**, 951.

25 M. P. Aldred, A. J. Eastwood, G. J. Richards, P. Vlachos, S. P. Kitney, M. O'Neill and S. M. Kelly, *Liq. Cryst.*, 2005, **32**, 1251.

26 The origin of the steps observed in Fig. 5 could be related to the artifacts of the analysis or equipment. DSC analysis of further samples have shown that this is the case.

27 H. Gallardo, F. R. Bryk, A. A. Vieira, T. E. Frizon, G. Conte, B. S. Souza, J. Eccher and I. H. Bechtold, *Liq. Cryst.*, 2009, **36**, 839.

28 H. Gallardo, G. Conte, P. A. Tuzimoto, B. Behramand, F. Molin, J. Eccher and I. H. Bechtold, *Liq. Cryst.*, 2012, **39**, 1099.

29 Collect, Enraf-Nonius, Nonius BV, Delft, The Netherlands, 1997–2000.

30 Z. Otwinowski and W. Minor, *Macromolecular Crystallography Part A*, 1997, vol. 276, p. 307.

31 A. Altomare, M. C. Burla, M. Camalli, G. L. Cascarano, C. A. Guagliardi, A. G. G. Moliterni, G. Polidori and R. Spagna, *J. Appl. Crystallogr.*, 1999, **32**, 115.

32 G. M. Sheldrick, *Acta Crystallogr., Sect. A: Found. Crystallogr.*, 2008, **64**, 112.

This journal is © The Royal Society of Chemistry 2013

J. Mater. Chem. C, 2013, **1**, 5583–5593 | **5593**